The Stability of Igneous Anhydrite: Experimental Results and Implications for Sulfur Behavior in the 1982 El Chichon Trachyandesite and Other Evolved Magmas

Article *in* Journal of Petrology · October 1987

DOI: 10.1093/petrology/28.5.781 · Source: NTRS

2 authors:

Michael R. Carroll
University of Camerino
118 PUBLICATIONS **6,497** CITATIONS
SEE PROFILE

Malcolm John Rutherford
Brown University
232 PUBLICATIONS **9,394** CITATIONS
SEE PROFILE

The Stability of Igneous Anhydrite: Experimental Results and Implications for Sulfur Behavior in the 1982 El Chichon Trachyandesite and Other Evolved Magmas

by MICHAEL R. CARROLL* AND MALCOLM. J. RUTHERFORD

Department of Geological Sciences, Brown University, Providence, Rhode Island 02912

(*Received 27 October 1986; revised typescript accepted 1 April 1987*)

ABSTRACT

Hydrothermal experiments on natural samples of trachyandesite and dacite bulk composition show that anhydrite ($CaSO_4$) may occur as a stable phenocryst phase at oxygen fugacities greater than or equal to 1·0 to 1·5 log f_{O_2} units above the Ni–NiO equilibrium. The dissolved sulfur concentration in anhydrite saturated melts from MnO–Mn_3O_4 buffered experiments decreases with decreasing temperature, from approximately 2300 p.p.m. S at 1025 °C to 250 p.p.m. S at 850 °C (all at 2 kb $P_{fluid} = P_{total}$). In FeS-saturated melts equilibrated at the Ni–NiO buffer and 2 kb pressure, the concentration of dissolved sulfur also decreases with decreasing temperature, varying from approximately 400 p.p.m. S at 1025 °C to less than 100 p.p.m. S at 850 °C. At NNO or lower f_{O_2}s, decreasing melt FeO content due to crystal fractionation may explain the observed decrease in sulfur solubility with decreasing temperature.

Sulfur solubility values equivalent to the approximately 0·6 wt. per cent S present in fresh bulk pumice samples from the 1982 eruptions of El Chichon volcano are not readily achieved under any reasonable combinations of pressure, temperature, and oxidation state. Dissolved sulfur contents approaching 0·6 wt. per cent might occur if the source regions of melts parental to the El Chichon trachyandesite were at an f_{O_2} several log units above the Ni–NiO equilibrium. Because such elevated oxidation states are far greater than the generally accepted values for mantle-derived partial melts we believe the high sulfur content of the El Chichon pumices is not a primary feature; it reflects reaction with sulfur enriched material at some unknown depth beneath the volcano. Published sulfur isotopic and petrologic data suggest that hydrothermally altered rocks similar to the pyrite- and anydrite-bearing lithic fragments found in the 1982 pumices could have provided a source of sulfur for crystallization of magmatic anhydrite. The anhydrite was an important source of sulfur for evolution of a sulfur-rich vapor phase during eruption of the magma.

Although many calc-alkaline dacites and rhyolites appear to attain oxidation states high enough to stabilize anhydrite, the characteristically low bulk sulfur contents of these rocks will limit anhydrite abundances to less than approximately 0·1 wt. per cent, assuming sufficient sulfur is present to achieve saturation. Such small amounts of a water soluble mineral could be easily removed by subaerial weathering processes, dissolved during vapor exsolution from a magma, or simply overlooked during routine petrographic examination.

INTRODUCTION

Anhydrite phenocrysts coexisting with rhyodacitic glass, and often included by other phenocrysts, are found in the trachyandesitic pumices from the 1982 eruptions of El Chichon

* Present Address: Division of Geological and Planetary Sciences, California Institute of Technology, Pasadena, California 91125

volcano, Chiapas, Mexico (Luhr *et al.*, 1984; Varekamp *et al.*, 1984). The large amounts of volcanically derived sulfate aerosols associated with the El Chichon eruptions have demonstrated the possible importance of anhydrite as a magmatic phase, and the potential influence of S-rich volcanic eruptions on the earth's climate (Rampino & Self, 1982; Sigurdsson, 1982; Devine *et al.*, 1984). From a petrologic viewpoint, the interesting questions are: (1) under what conditions does anhydrite become a stable magmatic phase; and (2) do these conditions for anhydrite stability account for the large amounts of S-rich aerosols associated with El Chichon eruptions, perhaps through changes in S-solubility.

The occurrence of anhydrite phenocrysts in the El Chichon 1982 tephras is unusual but not unique. Sigurdsson (pers. commun.) and Rose *et al.* (1984) have discovered anhydrite in the pre-1982 eruptive products of El Chichon volcano. In addition, Luhr (pers. commun.) has found a single inclusion of anhydrite in plagioclase from a hornblende trachyandesite from Cerro Lanza, approximately 130 km south-southeast of El Chichon. Anhydrite also occurs in the trachyandesites from the 1951 eruptions of Mt. Lamington, Papua New Guinea (Taylor, 1958; Arculus *et al.*, 1983), and Drexler (1982) reports primary anhydrite associated with a K_2O-rich dacitic to rhyolitic dike in the Miocene ore deposits of Julcani, Peru. Xenolithic anhydrite of contact-metamorphic or metasomatic origin, apparently more common than primary magmatic anhydrite, has been described from a number of localities, including El Chichon (Luhr, 1983), Mt Lamington (Taylor, 1958; Arculus *et al.*, 1983), Santorini volcano, Greece (Nicholls, 1971) and several Japanese volcanos (Yoshiki, 1932; Katsui, 1958; Yagi *et al.*, 1972). Whereas such occurrences may be important indicators of subvolcanic physiochemical conditions, the emphasis in this study is on the conditions necessary for anhydrite crystallization from a silicate melt. In this paper we present results from hydrothermal experiments designed to evaluate the effects of oxygen fugacity (f_{O_2}) and temperature (T) on the stability of anhydrite and the solubility of sulfur in evolved magmas.

EXPERIMENTAL AND ANALYTICAL METHODS

The majority of experiments reported in this paper were conducted using a finely ground (10 μm) sample of unweathered pumice from the 1982 eruption of El Chichon volcano (sample EC224, kindly provided by H. Sigurdsson; see Table 1). Some experiments were also done on a sample of Mt. St. Helens dacite (MSH18; see Table 1). Experimental conditions together with analytical and petrographic data are given in Tables 2 through 5. The experiments were conducted in both TZM (a titanium–zirconium–molybdenum alloy; Williams, 1968) and internally heated pressure vessels; quoted pressures and temperatures are estimated to be within 50 b and 10 °C of the true values. All experiments contained a fluid phase in which P_{H_2O} was close to total pressure.

Methods used in the Ni–NiO (NNO) and MnO–Mn_3O_4 (MNO) buffered experiments are identical to those of Carroll & Rutherford (1985), except that a smaller amount of FeS (3 wt. per cent) was added to the powdered starting compositions. Based on previous experience, the starting materials for NNO-buffered experiments were spiked with 5–7 wt. per cent Fe_2O_3 to compensate for Fe-loss to the platinum sample containers. Some of these experiments produced glasses with FeO heterogeneities on the order of ± 1 wt. per cent but because of the low sulfur concentrations in glasses from NNO buffered experiments, the effect of the FeO heterogeneities on S concentrations was within the error limits of microprobe analysis (see Table 2).

Experiments at intermediate oxygen fugacities between the NNO and MNO buffers were accomplished by introducing measured amounts of H_2 or CH_4 to the pressure vessel and generating the final pressure using Ar (e.g., see Popp *et al.*, 1984). For these experiments the

TABLE 1

Experimental starting materials

	(1) MSH-18	*(2) EC224*
SiO_2	62·81	55·81
TiO_2	0·60	0·86
Al_2O_3	17·89	18·16
FeO*	3·91	5·24
MgO	1·70	2·26
CaO	5·29	8·63
Na_2O	4·88	4·11
K_2O	1·29	2·61
MnO	0·07	0·24
P_2O_5	ND	0·48
SO_3	ND	0·025
Total	98·44	98·40
	CIPW norms	
Quartz	13·63	1·00
Albite	41·95	35·37
Anorthite	23·47	23·79
Orthoclase	7·74	15·68
Olivine	0·0	0·0
Hypersthene	9·38	7·53
Diopside	2·68	13·90
Ilmenite	1·16	1·66
Apatite	ND	1·07
Corundum	0·0	0·0

* Total iron as FeO.

(1) Bulk composition of Mt. St. Helens dacite, sample MSH-18, which is identical to SH-084 studied by Rutherford *et al.* (1985).

(2) Bulk composition of El Chichon trachyandesite, sample EC224, from A-1 pumice fall, 1982 eruption.

Compositions are from microprobe analyses of fused whole-rock samples. Analyses by Luhr *et al.* (1984) show El Chichon pumices also contain (wt. per cent) 0·13 per cent Cl, 0·11 per cent Sr, 0·08 per cent Ba, 1·24 per cent SO_3. During fusion the SO_3 in EC224 was lost.

charges were contained in small crimped Au tubes. The tubes containing the sample were paired with a second crimped Au tube containing a mixture of previously synthesized ilmenite solid solution (Il_{ss}) and magnetite solid solution (Mt_{ss}) and sealed in a larger Au or Pt tube for equilibration at the desired P and T. In some cases a third inner tube containing a second silicate charge was used. Upon completion of an experiment, microprobe analyses of the coexisting oxides provided an f_{O_2} value for the experiment (Buddington & Lindsley, 1964; Spencer & Lindsley, 1981). Oxygen fugacities were calculated from coexisting oxide compositions using the OXCALC2 program of Stormer (1983).

Experimental run products were examined in polished thin sections. Electron microprobe analyses were obtained using analytical procedures outlined in Carroll & Rutherford (1985) and Devine *et al.* (1984). Dissolved sulfur contents of experimental glasses were determined using a National Bureau of Standards soda–lime–silica glass containing 1150 p.p.m. sulfur. The decay-curve method of Nielsen & Sigurdsson (1981) was used to correct analyses of hydrous glasses for Na and K migration under the electron beam. All analyses were corrected for Na migration. Monitoring of count rates for K showed that only those glasses containing greater than approximately 3·0 wt. per cent K_2O required correction.

EXPERIMENTAL EQUILIBRIUM

The approach to equilibrium was investigated in several ways. To check on H_2 equilibration between buffer and charge in high f_{O_2} experiments (low f_{H_2}), charges of initially contrasting oxidation states were used. The low f_{O_2} charge consisted of a glass previously synthesized in a graphite–CH_4 buffered experiment; the other was a powder previously heated in air at 950 °C. These charges were run together with an MNO buffer assemblage at 2 kb total pressure and 1025 °C for 17 h. Analysis of the run products demonstrated equivalent sulfur contents, homogeneous melt (glass) chemistry, and identical phase assemblages (glass + Fe–Ti oxide + anhydrite) in the two charges. Several MNO and HM buffered experiments of 12 h duration (1025 °C, 2 kb) showed disequilibrium textures of FeS break-down and intergrowth with $CaSO_4$ + Fe-oxide. The sulfur contents of glasses from these experiments are approximately 15 per cent lower than values determined for similar experiments of 17 h duration. Longer duration experiments under identical conditions produced sulfur contents equal to that of the 17 h experiment. At lower temperatures where hydrogen diffusion through Pt container walls is slower (Chou, 1985), experiments of varying duration (18–68 h) produced consistent phase assemblages, melt compositions, and sulfur solubility values.

Approach to equilibrium in the experiments using synthetic Mt_{ss}–Ilm_{ss} mixtures as oxygen fugacity monitors is demonstrated by several observations. Preliminary experiments using crimped Au sample capsules showed that in some cases the crimps behaved like welds; water added to the sealed outer tube did not enter the silicate sample and resulting textures showed abundant relict plagioclase phenocrysts. Subsequent experiments using crimped Au sample tubes with pinholes at the top produced euhedral to subhedral crystalline phases with no relict plagioclase and apparent dissolved H_2O contents in accord with results previously obtained in this laboratory (Rutherford *et al.*, 1985). In order to test whether H_2 present in the outer tube equilibrated with the fluid phase in the inner sample tubes, several experiments were done using two sample tubes. Sulfur (1·0 wt. per cent) was added to one tube as FeS and to the other as $CaSO_4$. The run products of these experiments showed equivalent melt chemistries, phase assemblages, and dissolved sulfur contents independent of the form in which sulfur was added (e.g., experiments C141a, c and C142a, c Table 4). Additional evidence regarding equilibrium is provided by experiments C150 and C151, in which the Fe–Ti-oxide compositions indicate oxygen fugacities very close to the NNO and MNO buffer curves, respectively. The sulfur concentrations and phase assemblages produced in these experiments and in conventionally buffered experiments done at equivalent pressure and temperature are similar.

EXPERIMENTAL RESULTS

Experimental results concerning the effects of oxygen fugacity and temperature on the occurrence of anhydrite in hydrous trachyandesite are shown in Fig. 1. Tables 2 through 5 contain the experimental data on which this and following figures are based.

The solid symbols plotted on the MNO and NNO buffer curves in Fig. 1 represent experiments done at approximately 2 kb pressure. All MNO buffered experiments contain anhydrite + silicate melt (glass) + Fe–Ti-oxide + vapor (fluid) ± plagioclase, clinopyroxene, amphibole, and biotite. Several MNO buffered experiments contain traces of an iron-sulfide phase but these are always surrounded by thin rims of calcium sulfate. In contrast, the NNO buffered experiments contain similar silicate assemblages (at a given T) but pyrrhotite (or an FeS-rich immiscible melt) is the major sulfur-bearing phase. Experiments on samples of

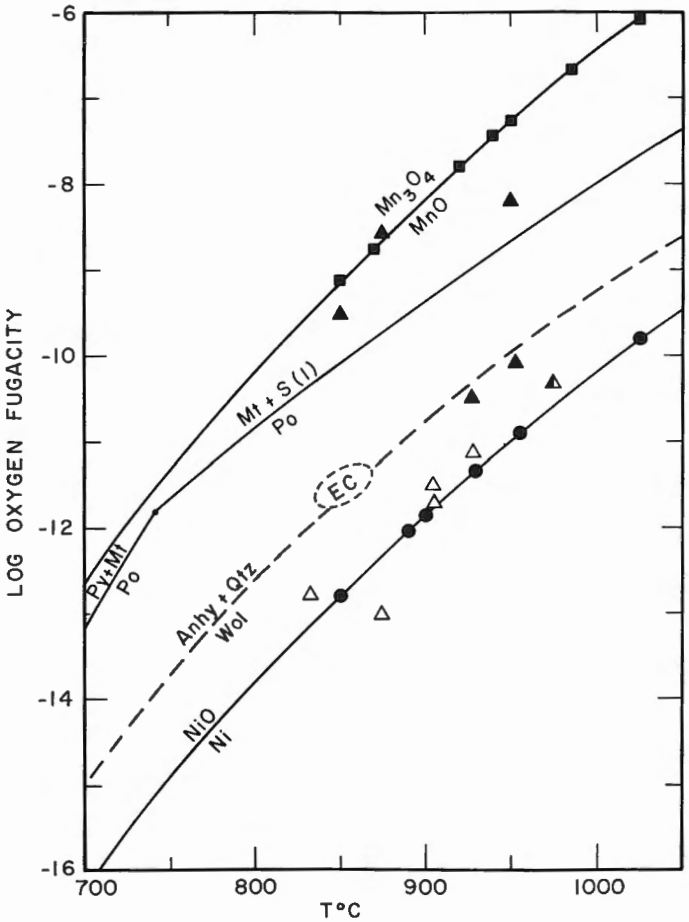

FIG. 1. Temperature–log f_{O_2} diagram showing experiments and calculated reactions relevant to anhydrite stability relations in magmas. All experiments plotted are at approximately 2 kb P_{fluid} ($=P_{total}$) except for C127a, C124a, and C126a (at approximately 1·1 kb; see Tables 2 and 3). Solid squares show anhydrite saturated experiments done using the MnO–Mn_3O_4 (MNO) buffer. Solid circles denote FeS saturated Ni–NiO (NNO) buffered experiments. Triangles show the T–f_{O_2} coordinates for experiments done using a mixed CH_4–Ar pressure medium and synthetic 2-oxide f_{O_2} indicators (discussed in text). Solid triangles indicate anhydrite present. Open triangles indicate experiments containing only an iron sulfide phase. The half-filled triangle indicates an experiment with mostly FeS but also several small $CaSO_4$ crystals. The dashed oval shows a T–f_{O_2} estimate for El Chichon 1982 pumices (Luhr *et al.*,1984). The dashed line above the NNO buffer curve indicates the estimated minimum f_{O_2} required to form anhydrite in the El Chichon trachyandesite. The solid line below the MNO buffer curve shows the upper f_{O_2} stability limit for pyrrhotite, which oxidizes to form magnetite + liquid sulfur (S(l)). Experiments at f_{O_2}s above this curve contain only anhydrite because S(l) is metastable relative to $CaSO_4$ when a Ca-bearing silicate melt is present. At temperatures below approximately 740°C oxidation of pyrrhotite will form pyrite (Py) + magnetite (Mt). Thermodynamic data were taken from Robie *et al.* (1978) where possible. Otherwise, data were taken from Stull & Prophet (1971; JANAF thermochemical tables). The NNO and MNO buffer curves were calculated using data of Huebner & Sato (1970).

Mt. St. Helens dacite and a Galapagos rift andesite indicate that anhydrite is not stable at NNO f_{O_2}s in other bulk compositions. The potential effects of magma bulk composition on anhydrite occurrence are discussed further in another section of this paper.

The curve immediately below the MNO-buffer curve on Fig. 1 shows the calculated f_{O_2}–T conditions where FeS, in the Fe–O–S system, breaks down by an oxidation reaction to form

TABLE 2

Ni–NiO and $MnO–Mn_3O_4$ buffered experiments

Run no.	*Buffer*	T(°C)	P(*kb*)	t(*h*)*	*Comp*†	*S*§(*p.p.m.*)	*Run products*‡
C72b	MNO	1027	2·06	16·0	MSH	2290–180	Gl, Ox, Anhy, (FeS)
C135a	MNO	985	2·02	20·0	EC	1940–110	Gl, Q, Ox, Anhy
C135b	MNO	985	2·02	20·0	EC-C	1860–60	Gl, Q, Ox, Anhy, Pl, (FeS)
C95c	MNO	950	1·95	33·5	EC	1460–210	Gl, Q, Ox, Anhy, (FeS)
M180	MNO	940	2·20	18·5	MSH	1290–140	Gl, Ox, Anhy
C102a	MNO	920	1·95	17·5	MSH	980–30	Gl, Ox, Anhy, (FeS)
C102b	MNO	920	1·95	17·5	EC	1150–60	Gl, Ox, Anhy, Pl
C103a	MNO	870	2·01	22·0	MSH	490–80	Gl, Ox, Anhy, Pl, Hb, (FeS)
C103b	MNO	870	2·01	22·0	EC	480–40	Gl, Ox, Anhy, Pl, Hb, Bt
C139a	MNO	850	2·07	32·0:24·0	EC-C	240–30	Gl, Ox, Anhy, Pl, Hb, Bt
C132a	MNO	950	1·12	25·5:21·5	MSH	680–90	Gl, Ox, Anhy, (FeS), Pl
C132b	MNO	950	1·12	25·5:21·5	EC	1140–200	Gl, Ox, Anhy, Pl, Px
C82a	NNO	1025	2·01	18·0	MSH	240–60	Gl, FeS
C82b	NNO	1025	2·01	18·0	EC	420–130	Gl, FeS, (Q)
C105a	NNO	955	2·02	20·5:17·5	MSH	210–30	Gl, FeS, Ox
C105b	NNO	955	2·02	20·5:17·5	EC	480–70	Gl, FeS, (Q), Ox
C85a	NNO	929	2·08	32·5	MSH	180–50	Gl, FeS
C85b	NNO	929	2·08	32·5	EC	300–60	Gl, FeS, (Q), Hb, (Pl)
C106a	NNO	900	2·08	24·0:18·0	MSH	200–100	Gl, FeS
C106b	NNO	900	2·08	24·0:18·0	EC	230–60	Gl, FeS, Hb
C97a	NNO	890	2·03	36·0:31·0	MSH	90–30	Gl, FeS, (Ox), Pl, Hb, Px
C97b	NNO	890	2·03	36·0:31·0	EC	110–30	Gl, FeS, Ox, Pl, Hb, Px
C99a	NNO	850	1·96	36·0:28·0	MSH	90–40	Gl, FeS, Ox, Pl, Hb
C99b	NNO	850	1·96	36·0:28·0	EC	100–30	Gl, FeS, Ox, Pl, Hb

* Run durations in hours. Numbers separated by ':' indicate total run time and time at final temperature, respectively, i.e. these are experiments in which the charge was initially held at near liquidus temperature and then cooled to the final temperature and held there for the time after the ':'.

† Starting compositions are MSH = Mt. St. Helens dacite, EC = El Chichon trachyandesite (see Table 1). Run numbers higher than C102 had sulfur added as 3 wt. per cent FeS. EC-C indicates sulfur added as 3 wt. per cent $CaSO_4$. Experiments numbered lower than C102 had approximately 10 wt. per cent FeS added. NNO—buffered experiments also had 5–7 wt. per cent Fe_2O_3 added to compensate for Fe-loss to the Pt sample containers.

‡ Run products include: Gl = glass, Q = fine grained quench crystals, Anhy = anhydrite, FeS = pyrrhotite or an FeS-rich immiscible sulfide liquid, Ox = iron–titanium oxide, Pl = plagioclase feldspar, Hb = amphibole, Px = calcium-rich pyroxene, Bt = biotite, ( ) = trace amount present.

§ Glass sulfur contents in p.p.m. S, number after '—' is 1σ variation in analyzed sulfur contents.

magnetite (Fe_3O_4) + liquid sulfur (S(l)). However, for Ca-bearing bulk compositions like the natural samples used in this study, S(l) is metastable relative to crystalline $CaSO_4$. As a result, anhydrite is a stable phase in MNO buffered experiments. At temperatures less than approximately 740 °C the phase relations in the system Fe–O–S indicate that pyrrhotite breaks down by oxidation to form pyrite (FeS_2) + magnetite. We have not conducted any experiments at temperatures low enough to stabilize pyrite but the experimental data of Brimhall *et al.* (1985) show that anhydrite is stable to at least 500 °C in Ca-bearing bulk compositions at f_{O_2}s in the pyrite stability field.

The coexistence of anhydrite and pyrrhotite (+silicate melt) in the trachyandesitic pumices from El Chichon suggests that there should be a field in T–f_{O_2} space where both phases may coexist. The reaction Po = Mt + S(l) shown in Fig. 1 provides an upper f_{O_2} limit for pyrrhotite stability. NNO buffered experiments, which contain only an iron sulfide phase, provide a lower boundary for the occurrence of anhydrite. Thus the stable coexistence of pyrrhotite + anhydrite requires oxidation states within the T–f_{O_2} region bounded by the NNO and Po–Mt–S(l) curves on Fig. 1. This region of T–f_{O_2} space includes conditions

TABLE 3

Hydrothermal experiments using 2-oxide f_{O_2} indicators

Run no.	T(°C)	P(*kb*)	t(*h*)*	*Comp*†	S‡(p.p.m.)	X_{usp}§	X_{ilm}	log f_{O_2}¶	*Run products*‖
C127a	974	1·16	49·0	EC	1070–210	42·3	76·8	−10·3 (0·3)	Gl, Q, FeS, (Anhy), r-Pl
C143a	953	2·03	34·0	EC	920–140	30·9	77·4	−10·1 (0·1)	Gl, Q, Ox, Anhy, Px, (Pl)
C110	950	1·99	16·0	EC	1150–180	8·3	52·5	− 8·2 (0·1)	Gl, Ox, Anhy, r-Pl
C141a	927	2·04	44·0:41·0	EC-C	290–80	39·5	82·9	−11·1 (0·2)	Gl, Ox, FeS, (Pl), Hb
C141c	927	2·04	44·0:41·0	EC	290–110	39·5	82·9	−11·1 (0·2)	Gl, Ox, FeS,
C142a	927	2·04	37·5:34·0	EC	700–120	35·6	75·6	−10·6 (0·3)	Gl, Ox, Anhy, Pl, (Hb)
C142c	927	2·04	37·5:34·0	EC-C	980–50	35·6	75·6	−10·6 (0·3)	Gl, Ox, Anhy, Pl, (Hb), (Px)
C126a	910	1·05	68·0	EC	150–40	48·1	81·2	−11·6 (0·5)	Gl, Ox, FeS, Pl, Px, r-Hb
C124a	910	1·05	42·2	EC	130–30	47·0	84·1	−11·8 (0·3)	Gl, Ox, FeS, Pl, Px
C146a	875	1·99	43·0:39·0	EC	70–20	49·5	91·0	−12·9 (0·2)	Gl, (Ox), FeS, Pl, Px, Hb
C151	875	2·05	54·5:46·5	EC	510–40	2·8	42·8	− 8·7 (0·3)	Gl, Ox, Anhy, Pl, Px, Hb
C152	850	2·07	47·0:42·0	EC	400–60	6·6	40·6	− 9·5 (0·4)	Gl, Ox, Anhy, Pl, Px, Hb, Bt
C150	833	2·05	54·5:46·5	EC	170–60	27·8	88·7	−12·8 (0·3)	Gl, Ox, FeS, Pl, Px, Hb, Bt

* Run times separated by ':' indicate total time and time at final temperature. Runs with only one time were put directly at the indicated temperature.

† Starting material for experiments was El Chichon trachyandesite with either 3 wt. per cent FeS added (EC), or 3 wt. per cent $CaSO_4$ added (EC-C).

‡ Glass sulfur contents, number after '—' is 1σ error.

§ Compositions, in mol per cent, of synthetic oxides used as oxygen fugacity monitors.

¶ Oxygen fugacity calculated from analysed compositions using calibrations of Spencer & Lindsley (1981). See text for additional details.

‖ Run products include: Gl = glass, Q = fine grained quench crystals, Ox = iron–titanium-oxides, Anhy = anhydrite, FeS = pyrrhotite or FeS-rich immiscible sulfide liquid, Pl = plagioclase feldspar, Px = Ca-rich pyroxene, Hb = amphibole, Bt = biotite, r- = relict phase, ( ) = trace amount present.

thought to be appropriate for the crystallization of a wide variety of calc-alkaline magmas (Carmichael & Nicholls, 1967; Haggerty, 1976; Whitney, 1984); however, no established buffer assemblages are available for use in hydrothermal experiments at oxygen fugacities between the NNO and MNO buffer curves.

The triangles plotted in Fig. 1 indicate experiments done with a $Mt_{ss} + Ilm_{ss}$ assemblage as an f_{O_2} monitor in a separate crimped tube adjacent to the tube(s) containing the silicate sample(s). All of these experiments were done using the El Chichon trachyandesite. The solid triangles indicate the presence of anhydrite; the open triangles indicate only FeS present. The half filled triangle at approximately 975 °C indicates an experiment containing mostly FeS but also a few small, anhedral crystals of anhydrite. The oxygen fugacity for each of these experiments was determined by analyzing the Fe–Ti oxide pairs which were in equilibrium with the fluid phase and the silicate starting material. By using available data on the relations between individual oxide composition, temperature and f_{O_2} (Buddington & Lindsley, 1964; Ghiorso & Carmichael, 1981; Spencer & Lindsley, 1981), and the fact that the temperature is known, it is possible to obtain an f_{O_2} estimate from the composition of each oxide in the Mt–Ilm pair. If equilibrium was achieved between the individual oxide phases, and between the oxides and the fluid phase, each oxide phase should indicate the same oxygen fugacity. Only experiments in which the indicated f_{O_2}s were within 0·5 log units were accepted as successful. Figure 2 schematically indicates how the experimental f_{O_2} is determined from analyses of the monitor assemblage. In this case the calculated temperature differs from the experimental temperature by approximately 75 °C but the uncertainty in calculated f_{O_2} is only $\pm 0{\cdot}3$ log units.

Table 5 lists the measured experimental temperatures and the f_{O_2}s indicated by the composition of each oxide phase. For comparison, the last two columns in Table 5 under the

TABLE 4

Experimental glass compositions

Sample	*C72b*	*C135a*	*C135b*	*C95c*	*M180*	*C102a*	*C102b*	*C103a*	*C103b*	*C139a*	*C82a*	*C82b*	*C105a*	*C105b*
T(°C)	1027	985	985	950	942	920	920	870	870	850	1025	1025	955	955
P(kb)	2·06	2·02	2·02	1·95	2·20	1·95	1·95	2·01	2·01	2·07	2·01	2·01	2·02	2·02
Buffer	MNO	MNO	MNO	MNO	MNO	MNO	MNO	MNO	MNO	MNO	NNO	NNO	NNO	NNO
Comp	MSH	EC	EC-C	EC	MSH	MSH	EC	MSH	EC	EC-C	MSH	EC	MSH	EC
SiO_2	69·66	60·14	61·56	67·08	69·05	67·11	62·94	69·91	67·92	74·23	64·75	56·80	63·61	55·33
Al_2O_3	17·89	19·05	18·81	19·60	18·11	18·32	19·99	17·28	17·65	16·30	18·09	19·00	17·14	18·71
FeO*	3·35	4·18	3·68	1·76	3·39	2·54	2·34	1·94	1·69	0·76	5·41	6·94	6·34	8·28
MgO	1·01	1·98	1·91	1·32	1·52	1·82	1·86	1·35	0·75	0·86	0·77	1·76	1·57	1·67
CaO	1·36	6·29	5·95	1·81	1·79	3·76	5·30	2·56	2·76	1·19	4·64	8·25	4·59	8·15
Na_2O	4·78	4·96	4·69	4·33	4·62	4·70	3·18	4·84	4·72	4·63	4·50	3·83	4·78	4·52
K_2O	1·53	2·63	2·52	3·11	1·14	1·09	3·18	1·53	4·01	1·71	1·32	2·13	1·31	2·19
TiO_2	0·42	0·64	0·75	0·10	0·36	0·61	0·77	0·53	0·31	0·26	0·51	0·82	0·60	0·65
MnO	0·01	0·13	0·13	0·49	0·02	0·06	0·04	0·06	0·06	0·05	0·01	0·11	0·06	0·05
P_2O_5	NA	NA	NA	0·36	NA	NA	0·38	NA	0·17	NA	NA	0·43	NA	0·46
H_2O	4·58	6·88	6·24	4·95	5·51	4·29	7·02	7·10	5·16	7·81	5·40	5·36	5·94	4·04
$\sqrt{\Sigma\sigma_i^2}$	0·50	0·44	0·91	0·49	0·77	0·44	0·61	1·58	0·50	1·14	0·83	1·70	0·72	1·81

TABLE 4 (*continued*)

Sample	*C85a*	*C85b*	*C97a*	*C97b*	*C99a*	*C99b*	*C127a*	*C143a*	*C141a*	*C141c*	*C142a*	*C142c*	*C126a*
T(°C)	929	929	890	890	850	850	974	953	927	927	927	927	910
P(kb)	2·08	2·08	2·03	2·03	1·96	1·96	1·16	2·03	2·04	2·04	2·04	2·04	1·05
Buffer	NNO	NNO	NNO	NNO	NNO	NNO	Ext	Ext	Ext	Ext	Ext	Ext	Ext
Comp	MSH	EC	MSH	EC	MSH	EC	EC	EC-C	EC	EC-C	EC	EC-C	EC
SiO_2	64·91	55·89	66·39	65·56	70·68	67·30	63·47	60·59	63·17	63·32	65·82	64·87	64·47
Al_2O_3	18·25	19·37	17·50	18·83	16·24	18·32	17·35	18·47	19·08	19·02	18·92	18·55	17·61
FeO*	4·42	8·47	4·36	2·50	2·39	1·84	3·01	4·64	2·28	2·34	1·38	2·01	4·14
MgO	1.83	1.48	1.02	0.40	0.66	0.38	1.80	0.87	1.11	1.47	1.49	1.24	0.90
CaO	4·42	6·89	4·10	3·02	2·79	2·56	5·14	5·46	5·10	4·77	3·75	4·19	2·87
Na_2O	4·08	4·56	4·84	4·96	4·94	4·56	3·97	5·38	5·22	4·96	4·60	4·85	5·03
K_2O	1·49	2·42	1·38	4·28	1·83	4·61	3·05	3·38	3·22	3·30	3·29	3·53	4·53
TiO_2	0·36	0·60	0·38	0·43	0·37	0·37	0·83	0·76	0·68	0·69	0·68	0·67	0·36
MnO	0·08	0·08	0·04	0·01	0·03	0·04	0·10	0·17	0·10	0·12	0·07	0·09	0·10
P_2O_5	NA	0·33	NA	0·03	NA	0·06	NA	NA	NA	NA	NA	NA	NA
H_2O	6·23	6·77	7·01	4·21	7·89	2·50	5·64	8·41	7·00	6·17	8·63	7·98	4·76
$\sqrt{\Sigma\sigma_i^2}$	0·57	0·65	2·30	0·85	1·94	0·76	0·76	1·02	0·99	1·28	0·66	0·46	0·42

All analyses given in wt. per cent oxide, recalculated on a water-free basis.

* Total iron as FeO.

H_2O indicates apparent water contents derived from difference between analysis totals and 100 per cent.

$\sqrt{\Sigma\sigma_i^2}$ = the square root of the sum of the squares of the standard deviation on each oxide analysed.

Each analysis represents the average of 5–11 different spots on the experimental charge.

NA = not analysed.

Starting compositions are: MSH, Mt. St. Helens dacite, and EC, El Chichon trachyandesite. Compositions with −C indicate that sulfur (1 wt. per cent) was added as calcium sulfate. Other compositions had sulfur added as FeS.

TABLE 5

Measured and calculated T *and* f_{O_2} *for unbuffered experiments*

	Measured‡			*OXCALC2*§	
Run no.	T(°C)	f_{O_2ilm}	f_{O_2mt}	T(°C)	*log* f_{O_2}
C127	974	− 9·8	−10·5	1062	− 8·8
C143	953	−10·1	−10·2	965	− 9·8
C110†	950	− 8·2	− 8·2	820	−10·4
C141	927	−10·9	−11·2	965	−10·3
C142	927	−10·2	−10·8	1027	− 9·0
C124*	910	−11·5	−12·1	1012	− 9·9
C126*	910	−11·1	−12·1	1068	− 9·0
C151†	875	− 9·0	− 8·4	720	−11·9
C146	875	−12·7	−13·1	880	−12·8
C152†	850	− 9·1	− 9·9	826	− 9·9
C150	833	−13·2	−12·6	800	−13·4

* Experiments in crimped tubes but no pinholes (see text).

† Experiments at oxygen fugacities beyond calibrations of Buddington & Lindsley (1964) and Spencer & Lindsley (1981).

‡ Columns under *Measured* indicate T measured during experiment and oxygen fugacities at that temperature as indicated by compositions of coexisting iron-titanium oxides used as an f_{O_2} monitor. Relations between ilmenite (ilm) and magnetite (mt) compositions and temperature were taken from interpolated data tabulated in Ghiorso & Carmichael (1981).

§ Columns under *OXCALC2* heading show T and f_{O_2} calculated from coexisting ilmenite and magnetite compositions using the OXCALC2 program of Stormer (1983).

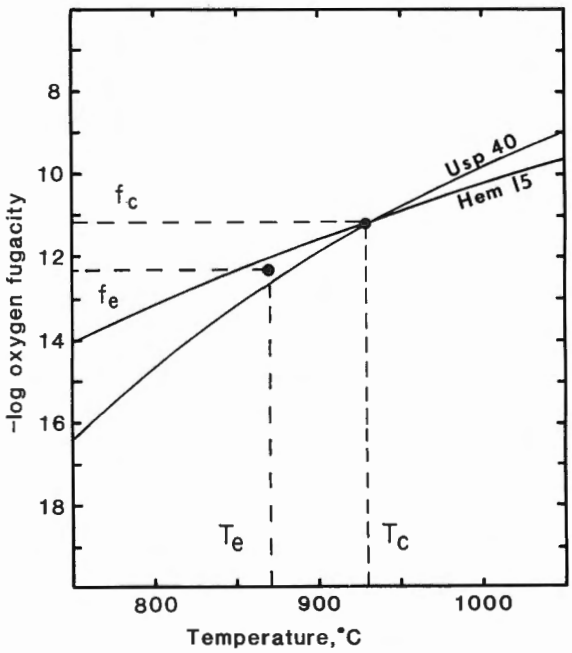

FIG. 2. Log f_{O_2}–Temperature diagram illustrating how oxygen fugacity is determined in experiments utilizing 2-oxide f_{O_2} monitor assemblage. T_e = measured experimental temperature; T_c = calculated temperature from compositions of coexisting oxides with composition 15 mol per cent hematite (Ilm_{ss}) and 40 mol per cent ulvospinel (Mt_{ss}); f_c = calculated f_{O_2} from oxide compositions; f_e = experimental f_{O_2} indicated by oxide compositions and the fact that the experimental temperature is known. In this case the indicated error in f_{O_2} is ±0·3 log units.

OXCALC2 heading contain the temperature and f_{O_2} calculated with the OXCALC2 program of Stormer (1983). Results for most experiments agree quite well within the errors inherent to the method (Spencer & Lindsley, 1981). Poor agreement is shown in several experiments at f_{O_2}s outside of the experimentally calibrated range, and several experiments for which the individual oxide compositions indicate f_{O_2}s separated by 0·5–1·0 log units. Because of the shallow angles of intersection between isopleths of Mt_{ss} and Ilm_{ss} composition (see Spencer & Lindsley, 1981, Fig. 4), the temperature calculated by the OXCALC2 program may differ by up to 100°C from the experimental temperature even though the estimated error in f_{O_2}, as indicated by the individual oxide phases, is less than $\pm 0{\cdot}5$ log units.

The results of experiments done with oxides as f_{O_2} indicators show that oxygen fugacities approximately 1·0–1·5 log f_{O_2} units above NNO are sufficient to stablilize anhydrite in the El Chichon trachyandesite. Oxidation states of this magnitude agree with the f_{O_2} estimates of Luhr *et al.* (1984) for the anhydrite-bearing pumices from El Chichon volcano, shown by the dashed oval marked EC on Fig. 1. Of more general interest however, is the large number of calc-alkaline volcanic rocks, especially those more silica-rich than andesite and those containing hornblende and/or biotite (Carmichael, 1967; Haggerty, 1976) that appear to have crystallized at f_{O_2}s high enough to stabilize anhydrite. This result is in contrast with the scarcity of anhydrite phenocrysts in calc-alkaline magmas.

The solubility of sulfur in an anhydrite saturated melt as function of T, f_{O_2}, etc. is a crucial factor affecting whether anhydrite will crystallize. Figure 3 shows the effects of temperature

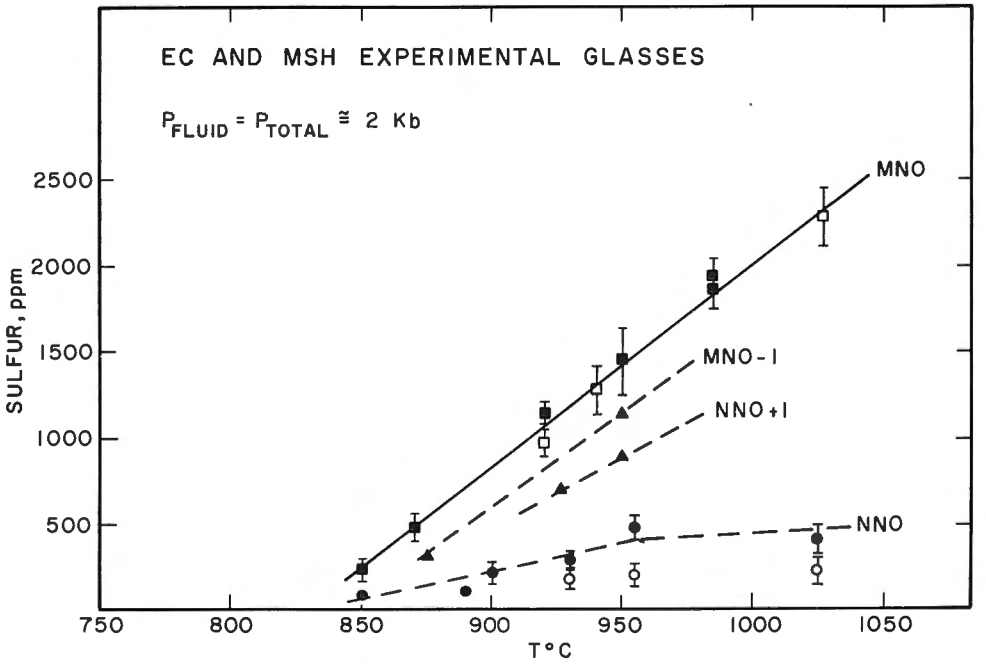

FIG. 3. Effect of temperature on sulfur content of experimental melts at 2 kb pressure. Solid squares denote MNO buffered experiments and solid circles denote NNO buffered experiments on the El Chichon trachyandesite. Open circles and squares indicate experiments done with Mount St. Helens dacite. Solid triangles show several experiments done at f_{O_2}s intermediate to these two buffers. All MNO buffered samples are saturated with anhydrite ($CaSO_4$) + Fe–Ti-oxide ± plagioclase, hornblende pyroxene (depending on temperature; see Table 2). NNO-buffered experiments are similar except that no $CaSO_4$ occurs; pyrrhotite or an FeS-rich immiscible sulfide liquid are the major sulfur-bearing condensed phases.

on sulfur solubility, as determined by electron microprobe analyses of glasses from experiments equilibrated at approximately 2 kb pressure and f_{O_2}s of the MNO and NNO buffers. All of the MNO buffered experiments (solid symbols = El Chichon trachyandesite, open symbols = Mt. St. Helens dacite) are anhydrite-saturated and the data define a fairly linear trend of sulfur solubility decreasing from approximately 2200 p.p.m. S at 1025 °C to 250 p.p.m. at 850 °C. This trend probably flattens out at temperatures lower than 850 °C, otherwise dissolved sulfur contents would approach zero at approximately 830 °C. The NNO experiments (solid circles = EC bulk composition) show broadly decreasing sulfur solubility with decreasing temperature, from approximately 400 p.p.m. S at 1025 °C to 100 p.p.m. S at 850 °C. However, this trend for NNO experiments is at least partly due to crystallization at lower temperatures and the resultant decrease in melt FeO content, which previous studies have shown to be correlated with decreasing sulfur solubility (Haughton *et al.*, 1974; Mathez, 1976; Carroll & Rutherford, 1985). The importance of melt FeO content in affecting sulfur solubility in sulfide saturated melts is also demonstrated by the lower sulfur contents of experiments done on the dacite starting composition, denoted by the open circles on Fig. 3 (see Table 4 for melt composition).

A comparison of results from NNO and MNO buffered experiments shows that the more oxidizing conditions favor higher sulfur solubility, with the difference being greater at higher temperatures. At temperatures less than 850 °C, the solubility of sulfur is relatively low and differs by only 150 p.p.m. in anhydrite and FeS saturated melts. At 1025 °C, sulfur solubility increases from approximately 450 p.p.m. at NNO to 2200 p.p.m. at MNO. The two dashed lines on Fig. 3, labeled MNO − 1 and NNO + 1, indicate sulfur solubility values from experiments with f_{O_2} between the MNO and NNO buffer curves. The −1 and +1 refer to log f_{O_2} units, relative to the indicated buffer curves. These curves should be considered as approximations only because of the limited amount of data.

The combined effects of oxygen fugacity and temperature on sulfur solubility in hydrous Mt. St. Helens and El Chichon composition melts are shown in Fig. 4. The plotted experiments were all done at 2 kb pressure. The GCH, FMQ, and MNO (1025 °C) experiments are taken from Carroll & Rutherford (1985). Sulfur solubility values at NNO, MNO (950 °C, 900 °C) and intermediate f_{O_2}s are taken or interpolated (MNO, 900 °C) from experiments reported in this paper (Tables 2 and 3). The GCH, FMQ and NNO buffered experimental glasses all contain approximately 5 wt. per cent FeO and 250 p.p.m. S; higher FeO contents would slightly increase sulfur solubility at these f_{O_2}s. The isotherms for 1025, 950, and 900 °C show that higher sulfur solubility is favored by higher temperatures and higher oxidation states when f_{O_2}s above the Ni–NiO equilibrium prevail. The isotherms have not been drawn to extend to f_{O_2}s below NNO because sulfur solubility at these lower f_{O_2}s will depend more on melt FeO content than on temperature. Since lower temperatures generally correlate with lower melt FeO contents and more differentiated melts, the effects of composition and temperature on S-solubility are difficult to separate in subliquidus runs.

The relation between dissolved sulfur and melt FeO content in sulfide saturated experiments at 2 kb pressure is shown in Fig. 5. Sulfur contents vary from 100 p.p.m. at 2 wt. per cent FeO to 700 p.p.m. at 8·5 wt. per cent FeO. The solid triangles indicate NNO-buffered experiments (850–1025 °C) from this study. The open circles show sulfur solubility values from FMQ buffered experiments done at 1025 °C (Carroll & Rutherford, 1985). The curve drawn through the data was fitted by eye. For comparison, the dashed curve labeled HRS is from the work of Haughton *et al.* (1974) on sulfur solubility in basaltic melts at 1250 °C and 1 atm. pressure.

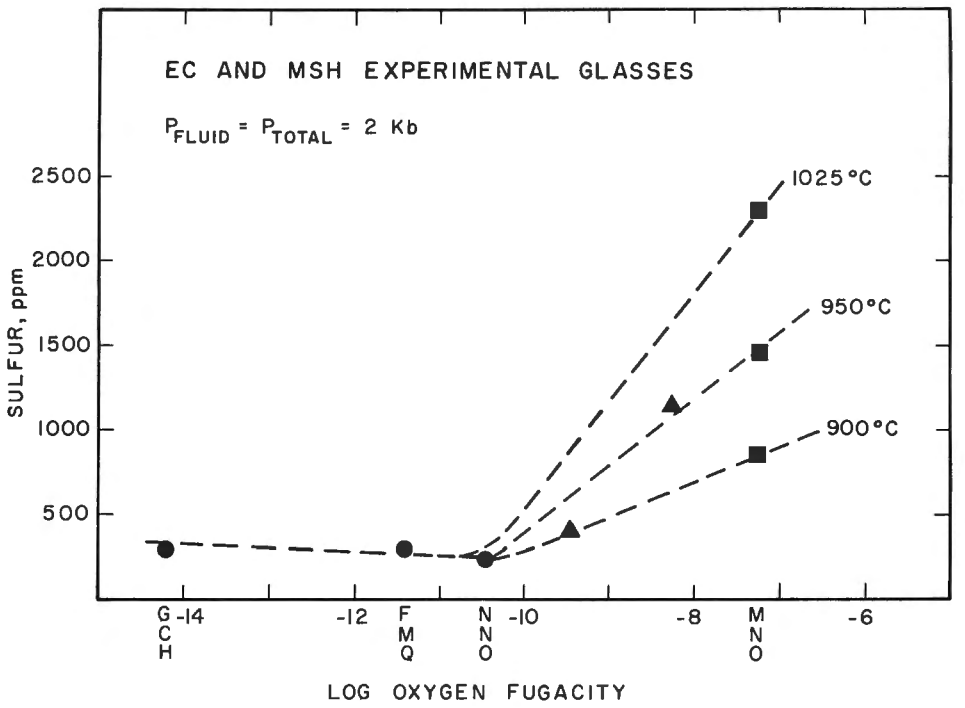

FIG. 4. Sulfur concentrations as a function of experimental oxygen fugacity. Solid circles show graphite–CH_4 (GCH; Eugster & Skippen, 1967), QFM, and MNO (1025 °C) buffered experiments from Carroll & Rutherford (1985). All other experiments from this study. Solid squares denote MNO buffered experiments. Triangles denote experiments done with Ar–CH_4 mixtures and 2-oxide f_{O_2} indicators. Isotherms at 950 and 900 °C are not drawn to extend to oxygen fugacities below NNO but they will lie slightly below the 1025 °C isotherm; how far below will depend on melt FeO contents.

DISCUSSION

Sulfur mass balance in magmas

Whole-rock sulfur abundances will be an important factor affecting the occurrence of phenocrystic anhydrite in magmas, and the results of this study provide constraints on the amount of sulfur required for anhydrite saturation. Even if P, T, f_{O_2}, and magma composition favor crystallization of anhydrite, there must be enough sulfur present to saturate the melt. Undegased basaltic glasses typically contain between 800 and 1500 p.p.m. dissolved sulfur (Moore & Fabbi, 1971; Czamanske & Moore, 1977; Mathez, 1976) and their oxidation states are usually 1 to 2 $\log f_{O_2}$ units below the NNO buffer curve (Carmichael & Ghiorso, 1986; Basaltic Volcanism Study Project, 1981). More evolved magmas are often more highly oxidized but their sulfur contents tend to be lower than those observed in basalts. If we consider andesites as the least differentiated magmas likely to achieve oxidation states within the anhydrite stability field, their typical sulfur contents of less than 1000 p.p.m. S (Gill, 1981; Anderson, 1974) correspond to a maximum of approximately 0·35 wt. per cent potential $CaSO_4$. Most magmas characterized by oxidation states within the anhydrite stability field are dacitic or rhyolitic in composition and contain several hundred p.p.m. S at most (e.g., Devine *et al.*, 1985). The experiments reported in this paper indicate that sulfur concentrations of 100–200 p.p.m. are required to saturate

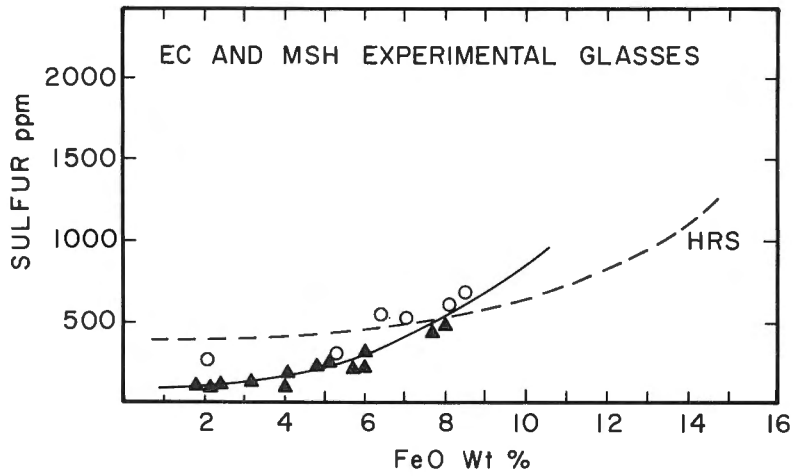

FIG. 5. Diagram showing the relation between melt FeO content and sulfur concentration in hydrothermal experiments done at 2 kb fluid pressure. Solid triangles indicate Ni–NiO buffered experiments (850–1025 °C). Open circles indicate fayalite–magnetite–quartz buffered experiments, all done at 1025 °C. Dashed line labeled HRS is from experimental data of Haughton *et al.* (1974) on sulfur solubility in dry basaltic melts at 1 atm., 1250 °C.

anhydrite at temperatures in the 850 °C range. It is thus possible that oxidation of a magma to f_{O_2}s within the anhydrite stability field could actually produce a sulfur undersaturated melt. Even if sufficient sulfur is present to saturate anhydrite the observed low sulfur contents of evolved magmas will severely limit the abundance of magmatic anhydrite.

Many dactic to rhyolitic calc-alkaline magmas lack groundmass pyrrhotite in equilibrium with the host liquid, although pyrrhotite commonly occurs as inclusions within silicate and oxide phenocrysts in the same sample. The restricted occurrence of phenocrystic pyrrhotite in silicic volcanics could indicate that the early crystallized sulfide has been oxidized to sulfate, and either the amount of sulfur present is insufficient to saturate anhydrite, or else only trace amounts of anhydrite are produced. The rarity of groundmass pyrrhotite in silicic volcanics may also be related to production and evolution of an H_2O-rich fluid phase with high partial pressures of H_2S and SO_2 (see Whitney & Stormer, 1983; Whitney, 1984). Sulfides trapped in phenocrysts would be isolated from this process but the rest of the magma's sulfur could be quickly depleted in order to provide the sulfur required for the equilibrium fluid composition. Fluid saturation and loss of H_2 from a magma may be important in producing the elevated f_{O_2}s observed in many dacites and rhyolites (Carmichael & Nicholls, 1967; Czamanske & Wones, 1973; Mason, 1978; Chivas, 1981; Candella, 1986); if so, the loss of sulfur to an evolving and escaping fluid might explain the lack of anhydrite in magmas with f_{O_2}s that appear to be within the anhydrite stability field.

Temperature and anhydrite stability

The experiments reported in this paper demonstrate that anhydrite may coexist with trachyandesite to rhyolite melt over the temperature range 1040–800 °C. Anhydrite alone, at 1 atm. pressure, is stable to approximately 1200 °C where it decomposes to $CaO + SO_3$ (Gay, 1965). In natural systems the effects of temperature on magmatic sulfur contents will influence the appearance and abundance of anhydrite. However, temperature and melt composition are interdependent variables in natural systems because decreasing tempera-

ture promotes crystallization and changes in melt chemistry. As previously discussed in reference to the NNO-buffered experiments in Figs. 3 and 5, decreasing sulfur solubility is correlated with decreasing melt FeO content at oxidation states below NNO, where sulfur is mainly present as sulfide dissolved in the melt. These observations suggest that the temperature at which a magma becomes sufficiently oxidized to stabilize anhydrite will affect the amount of sulfur available for anhydrite formation. Oxidation of higher temperature basaltic or andesitic magmas, because of their higher sulfur contents, would produce greater amounts of anhydrite than would be expected from oxidation of dacitic or rhyolitic compositions.

MNO buffered experiments show that decreasing temperature is also accompanied by decreasing dissolved sulfur contents in anhydrite-saturated melts. However, the reasons for this behavior are not clear. If sulfur dissolves as SO_4^{2-} at high f_{O_2}s, then by analogy with CO_2 solubility as CO_3^{2-} (Fine & Stolper, 1985) we might expect lower sulfate solubility in more silicic melts. The activity of alkali metals or alkaline earth elements may also affect sulfate solubility in a silicate melt, as suggested by thermochemical data for reactions of the type

$$M_xO + SO_3 = M_xSO_4,$$

where M_xO represents a metal oxide. Unfortunately we are unable to comment on the importance of these mechanisms because our solubility data do not cover a significantly diverse range of melt compositions. Further work is needed to evaluate the solubility mechanisms of oxidized sulfur species, nevertheless the observed decrease in sulfur solubility (as sulfate) with decreasing temperature could be an important factor influencing the occurrence of anhydrite and the amount of sulfur contained in evolved magmas.

Pressure and anhydrite stability

A possible replacement for anhydrite in high pressure magmas containing sulfate sulfur is sulfate-bearing scapolite, a common high-grade metamorphic mineral (Shaw, 1960; Lovering & White, 1964). For the simple system CaO–Al_2O_3–SiO_2–SO_3, the experimental results of Newton & Goldsmith (1976) show sulfate-scapolite replacing the assemblage anorthite + anhydrite at 960 °C at 5 kb and 820 °C at 10 kb. Although these experiments did not involve a melt phase, they suggest that the presence of sulfate sulfur in high pressure magmas may result in the crystallization of scapolite rather than anhydrite. The few documented occurrences of sulfate-rich scapolite in igneous parageneses have also been interpreted to represent crystallization under elevated P, T conditions and oxygen fugacities near or above the NNO buffer (Bovin & Camus, 1981; Goff *et al.*, 1982).

A second means by which pressure may influence anhydrite stability concerns pressure induced changes in sulfur solubility. With oxidation states at or below the FMQ buffer, increasing pressure between 1 and 2 kb has relatively little effect on the sulfur concentration in sulfide saturated hydrous dacite melts (Carroll & Rutherford, 1985). In contrast, sulfur solubility in the same dacite saturated with anhydrite increases from 1500 p.p.m. at 1 kb to 3000 p.p.m. at 2·9 kb (MNO buffer, 1025 °C). Experiments at 950 °C from this study also show a positive correlation between pressure and sulfur solubility (runs C95c, 1960 p.p.m., 1·95 kb and C132b, 680 p.p.m., 1·1 kb; see Table 2). These data require that high pressure magmas will need to dissolve more sulfur than low pressure magmas in order to saturate anhydrite, assuming the experiments are applicable to natural systems. This effect could prohibit anhydrite saturation in magmas with small amounts of sulfur, or at least delay saturation until sufficiently low pressures are achieved.

Magma composition and sulfate minerals

Data on anhydrite occurrence in magmas of other than trachyandesitic composition are not available, yet it is informative to consider how melt composition may affect the occurrence of sulfate minerals. The most common igneous sulfates, nosean ($Na_8Al_6Si_6O_{24}SO_4$), and hauyne ($(Ca, Na)_{4-8}Al_6Si_6O_{24}(S, SO_4)_{1-2}$) are generally restricted to silica-undersaturated rocks (Deer *et al.*, 1963). Nosean is found mainly in phonolites and nepheline syenites while hauyne occurs in magmas ranging from alkali-olivine basalt to trachyte to nephelenite (Carmichael *et al.*, 1974; Tracy & Hummel, 1981). Studies of these types of rocks do not indicate anomalously high sulfur contents or formation under unusually high oxygen fugacities (Schneider, 1970; Carmichael *et al.*, 1974; Ueda & Sakai, 1984).

As suggested by Stormer & Carmichael (1971) the formation of nosean (or hauyne) might be represented by the reaction:

$$Na_8Al_6Si_6O_{24}SO_4 + Fe_3O_4 + 16SiO_2 = FeS + 2NaFeSi_2O_6 + 6NaAlSi_3O_8 + 2O_2$$

This reaction indicates that even at constant f_{O_2}, decreased SiO_2 activity favors crystallization of nosean at the expense of FeS. Similarly, the paragenesis of anhydrite might be represented by the reaction:

$$3CaSiO_3 + 3FeS + 13/2O_2 = 3CaSO_4 + Fe_3O_4 + 3SiO_2$$

The position of this reaction in T–f_{O_2} space, with the activities of the condensed phases set at unity, is shown by the dashed curve in Fig. 6. The location of this reaction also coincides closely with the lower f_{O_2} boundary for anhydrite stability drawn on Fig. 1. As in the example for nosean, this reaction shows that anhydrite may be created at the expense of FeS simply by decreasing the activity of SiO_2 in the melt. The position of the wol–FeS–anhy–mt–qtz reaction in Fig. 6 was calculated with $a_{SiO_2} = 1$; lower SiO_2 activities will move the curve to lower f_{O_2} at a given temperature (by 6/13 of a log f_{O_2} unit per log unit decrease in SiO_2 activity, with all other activities held constant).

Although the activity of $CaSiO_3$ in natural melts is difficult to estimate, it will clearly be less than unity. By recasting the anhydrite-forming reaction above into log activity terms, it can be shown that for each log unit decrease in a_{CaSiO_3}, the curve plotted in Fig. 6 will move up by approximately 0·5 log f_{O_2} units (assuming anhydrite, FeS, and magnetite are present). The dotted curve in Fig. 6 is calculated for $a_{CaSiO_3} = 0{\cdot}01$. In terms of CIPW normative components, the wollastonite content of normative diopside is a measure of the Ca present in excess of that needed to form normative feldspar. This observation can be used to predict that magmas with normative diopside will crystallize anhydrite at lower oxygen fugacities than magmas with low or absent normative diopside, other factors being equal. Quantification of these relations would require further experimentation on more diverse melt compositions, but it is interesting to note that the anhydrite-bearing magmas of both El Chichon and Mt. Lamington are distinguished by alkali-rich bulk compositions.

Application to El Chichon

The recent (1982) eruptions of anhydrite-bearing trachyandesite at El Chichon volcano have focused attention on the possible relations between sulfur-rich volcanic eruptions and global climatic variations. For a number of historical eruptions, Devine *et al.* (1984) have used estimated eruptive volumes and analyses of sulfur concentrations in both melt inclusions and their coexisting matrix glasses to demonstrate a positive correlation between

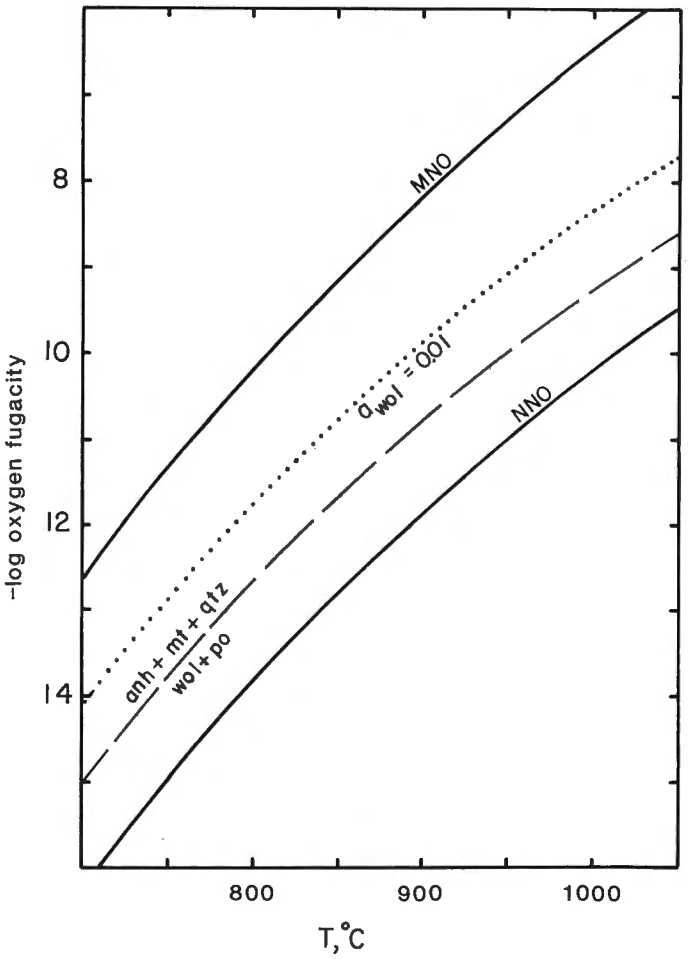

FIG. 6. Temperature–f_{O_2} relations for reactions possibly involved in the formation of magmatic anhydrite. Heavy solid lines show Ni–NiO (NNO) and MnO–Mn_3O_4 (MNO) buffer curves for reference. Dashed curve is for the reaction which involves wollastonite (wo), anhydrite (anhy), FeS (po), SiO_2 (qtz), and magnetite (mt); all condensed phases at unit activity, see text for discussion. The dotted curve shows the position of the same reaction when the activity of $CaSiO_3$ is 0·01.

volcanic sulfur emissions and global mean temperature decreases. At El Chichon, the sulfur yield to the atmosphere as measured by airborn and satellite observations (Hofmann & Rosen, 1983; Krueger, 1983; Mroz *et al.*, 1983) was two orders of magnitude greater than that indicated by considering the volume of erupted material and the difference in sulfur content between melt inclusions and matrix glass (Devine *et al.*, 1984; Luhr *et al.*, 1984). The results of this study provide new information regarding the origin of the high sulfur concentrations in the 1982 El Chichon trachyandesite and the associated volcanic gases emitted to the atmosphere. As shown by our experiments, magmatic anhydrite does not require extreme conditions to crystallize; it's rarity is more a reflection of the low sulfur concentrations found in most igneous rocks.

Estimates of the total sulfur budget at El Chichon, including sulfur in pumice deposits as well as sulfur lost to the atmosphere, require a magma with approximately 1·04 wt. per cent S,

assuming all sulfur was derived from the volume of erupted material (Varekamp *et al.*, 1984). Some of the sulfur may have come from degasing of unerupted material, but the $0{\cdot}63 \pm 0{\cdot}15$ wt. per cent S present in fresh pumice samples (Prol *et al.*, 1982) should be considered as a lower limit for the magmatic sulfur content. Experimental data from this study and from a number of others (Haughton *et al.*, 1974; Katsura & Nagashima, 1974; Mysen & Popp, 1981; Wendlandt, 1982; Carroll & Rutherford, 1985) show that it would be extremely difficult to dissolve more than half of 1 wt. per cent S in a magma under any combination of P, T, and f_{O_2} conditions. Extrapolation of the data of Carroll & Rutherford (1985) for sulfur solubility in hydrous anhydrite-saturated dacite (MNO buffer, 1025 °C, 1–2·9 kb) suggests that sulfur contents near 0·5 wt. per cent S might be achieved at pressures of 5 kb or more. However, there is considerable uncertainty in a straight-line extrapolation of the data to higher pressures; in addition, relative to conditions considered appropriate for the mantle source regions of calc-alkaline magmas (Basaltic Volcanism Study Project, 1981; Gill, 1981), the experiments are highly oxidizing and water-rich (vapor saturated). Mineral chemistries in the El Chichon pumices also do not support extremely oxidizing (near MNO) conditions in the magma prior to eruption. Together, these observations suggest that interaction between trachyandesite magma and sulfur-rich material at depth is required to account for the high sulfur content of the erupted pumices.

The sulfur isotopic measurements of Rye *et al.* (1984) on El Chichon pumices suggest that the magma's high sulfur content cannot be due to reaction with marine evaporites known to underlie the volcano. The $+5{\cdot}8$ per mille $\delta^{34}S$ value estimated for the El Chichon magma + vapor phase is higher than the 0 ± 3 per mille value considered typical for 'mantle' sulfur but it agrees well with reported $\delta^{34}S$ values of $+5$ to $+7$ per mille for subduction-related basalts and andesites from Japan (Ueda & Sakai, 1984). Rye *et al.* (1984) suggest that altered oceanic crust in the underlying Cocos Plate could have provided a source of heavy sulfur for partial melts parental to the El Chichon trachyandesite. Because available sulfur solubility data show that it would be difficult to produce a melt containing as much dissolved sulfur as occurs in the El Chichon pumices we favor a magmatic history involving interaction between primary trachyandesite magma (500–1000 p.p.m. S) and sulfur enriched subvolcanic rocks such as the pyrite and anhydrite-bearing altered lithic fragments observed in the 1982 pumices. A scenario involving hydrothermal alteration of subvolcanic rocks, later reaction between trachyandesite magma and the altered materials, and crystallization of anhydrite to produce a sulfur-enriched magma would be consistent with sulfur isotopic, petrologic and experimental (solubility) data.

CONCLUSIONS

In the beginning of this paper we addressed two questions concerning: (a) the conditions required to stabilize anhydrite as a magmatic phase; and (b) whether these conditions explain the large amounts of sulfur gases associated with the 1982 eruptions of anhydrite-bearing pumices at El Chichon volcano. The answers to these questions, and several other conclusions regarding the behavior of sulfur in andesitic or more highly evolved magmas can be summarized as follows:

(1) Experimental results from this study show that anhydrite, as well as minor amounts of FeS, may be stable in the El Chichon bulk composition at oxidation states of 1·0 to 1·5 log f_{O_2} units above the NNO buffer curve. Oxygen fugacities of this magnitude agree with the f_{O_2} estimates made by Luhr *et al.* (1984) on the basis of mineral chemistries observed in El Chichon pumice samples. At f_{O_2}s above NNO + 2·5 to 3 log units, all FeS would be oxidized to form anhydrite. This constitutes an upper f_{O_2} limit for the El Chichon magma.

(2) Prior to eruption the melt phase of the El Chichon magma contained 200–300 p.p.m. dissolved sulfur, based on melt inclusion analyses. The bulk magma contained a minimum of 0·6 wt. per cent S. Experimental sulfur solubility data from this study, and others (Haughton *et al.*, 1974; Mysen & Popp, 1981; Wendlandt, 1983; Carroll & Rutherford, 1985) show that it would be extremely difficult to produce a melt with 0·6 wt. per cent dissolved sulfur. This suggests that the high sulfur content of the El Chichon trachyandesite is not a primary magmatic feature but rather, it is the result of sulfur addition from sources external to the magma. Reaction between trachyandesite magma and hydrothermally altered and sulfur-rich subvolcanic material like the lithic fragments found in the El Chichon pumices could have provided a source of sulfur for anhydrite precipitation. The depth at which this occurred would have to be within the amphibole stability field because anhydrite inclusions occur in the rims of amphibole phenocrysts. When the anhydrite-bearing El Chichon magma achieved vapor saturation the anhydrite phenocrysts would have provided a significant source of sulfur for evolution of a sulfur-rich fluid phase. In this way the presence of abundant phenocrystic anhydrite would have been an important factor contributing to the large amounts of sulfurous gases emitted to the atmosphere.

(3) Anhydrite-saturated melts from MNO-buffered experiments at 2 kb pressure show sulfur solubility decreasing with decreasing temperature, from 2300 p.p.m. S at 1025 °C to 250 p.p.m. S at 850 °C. NNO-buffered experiments also show decreasing sulfur solubility with decreasing temperature, although part of this effect is probably due to decreased melt FeO content caused by crystallization at lower temperatures.

(4) The apparent rarity of anhydrite in calc-alkaline volcanic rocks which appear to have f_{O_2}s within the anhydrite stability field may be partly due to their low sulfur concentrations (100–500 p.p.m. S). This factor, as well as the ease with which anhydrite can be dissolved by subaerial weathering processes may limit the preservation of magmatic anhydrite in the geologic record.

(5) The effects of melt composition on anhydrite stability need further investigation. One important parameter appears to be the amount of Ca + Na + K present in excess of that required to form normative feldspar. Theoretical considerations suggest that corundum-normative melts would require oxidation states higher than those reported in this study for stabilizing anhydrite.

ACKNOWLEDGEMENTS

Financial support for this work was provided by grants NSG-7589 and EAR-85-00795. Microprobe analytical work was supported by EAR-84-15794 and a grant from the Keck Foundation to Brown University. The manuscript benefited from reviews by J. Luhr and M. Dungan. The comments of P. Hess, L. P. Gromet, G. Porus, M. Rutter, and D. Weis at various times during preparation of this manuscript are also appreciated.

REFERENCES

Anderson, A. T., 1974. Chlorine, sulfur, and water in magmas and oceans. *Bull. geol. Soc. Am.* **85,** 1485–92.

Arculus, R. J., Johnson, R. W., Chappell, B. W., Mckee, C. O., & Sakai, H., 1983. Ophiolite contaminated andesites, trachybasalt, and cognate inclusions of Mount Lamington, Papua New Guinea: anhydrite-bearing lavas and the 1951 cumulodome. *J. Volcanol. geotherm. Res.* **18,** 215–47.

Basaltic Volcanism Study Project, 1981. *Basaltic Volcanism on the Terrestrial Planets.* New York: Pergamon Press Inc.

Boivin, P., & Camus, G., 1981. Igneous scapolite-bearing associations in the Chaine des Puys, Massif Central (France) and Atakor (Hoggar, Algeria). *Contr. Miner. Petrol.* **77,** 365–74.

Brimhall, G. H., Agee, C., & Stoffregen, R., 1985. The hydrothermal conversion of hornblende to biotite. *Can. Miner.* **23,** 369–79.

Buddington, A. F., & Lindsley, D. H., 1964. Iron–titanium oxide minerals and synthetic equivalents. *J. Petrology*, **5**, 310–57.

Candella, P. A., 1986. The evolution of aqueous vapor from silicate melts: effects on oxygen fugacity. *Geochim. cosmochim. Acta*, **50**, 1205–11.

Carmichael, I. S. E., 1967. The iron–titanium oxides of salic volcanic rocks and their associated ferromagnesian silicates, *Contr. Miner. Petrol.* **14**, 36–44.

—— Ghiorso, M. S., 1986. Oxidation–reduction relations in basic magma: a case for homogeneous equilibria. *Earth planet. Sci. Lett.* **78**, 200–10.

—— Nicholls, J., 1967. Iron–titanium oxides and oxygen fugacities in volcanic rocks. *J. geophys. Res.* **72**, 4665–87.

—— Turner, F. J., & Verhoogen, J., 1974. *Igneous Petrology*. New York: McGraw Hill.

Carroll, M. R., & Rutherford, M. J., 1985. Sulfide and sulfate saturation in hydrous silicate melts. *Proc. 15th Lunar Planet. Sci. Conf., J. geophys. Res.* **90**, C601–12.

Chivas, A. R., 1981. Geochemical evidence for magmatic fluids in porphyry copper mineralization, Part 1. *Contr. Miner. Petrol.* **78**, 389–403.

Chou, I. M., 1985. Permeability of precious metals to hydrogen at 2 kb and the quantification of the oxygen buffer technique. *EOS Trans. Am. geophys. Union*, **66**, 407.

Czamanske, G. K., & Moore, J. G., 1977. Composition and phase chemistry of sulfide globules in basalt from the mid-Atlantic ridge rift valley near 37°N latitude. *Bull. geol. Soc. Am.* **88**, 587–99.

—— Wones, D. R., 1973. Oxidation during magmatic differentiation, Finmarka Complex, Oslo area, Norway: Part 2, the mafic silicates. *J. Petrology*, **14**, 349–80.

Deer, W. A., Howie, R. A., & Zussman, J., 1963. Framework silicates. In: *Rock Forming Minerals*, Vol. 4. London: Longmans, Green and Co. 289–303.

Devine, J. M., Sigurdsson, H., Davis, A. N., & Self, S., 1984. Estimates of sulfur and chlorine yield to the atmosphere from volcanic eruptions and potential climatic effects. *J. geophys. Res.* **89**, 6309–25.

Drexler, J. W., 1982. Mineralogy and geochemistry of Miocene volcanic rocks genetically associated with the Julcani Ag–Bi–Pb–Cu–Au–W deposit, Peru: Physiochemical conditions of a productive magma body. *PhD dissertation, Mich. Tech. Univ.*, 259 pp.

Eugster, H. P., & Skippen, G. B., 1967. Igneous and metamorphic reactions involving gas equilibria. In: Abelson, P. H. (ed.) *Researches in Geochemistry*, Vol. 2. New York: Wiley, 492–531.

Fine, G., & Stolper, E., 1985. The speciation of carbon dioxide in sodium aluminosilicate glasses. *Contr. Miner. Petrol.* **91**, 105–21.

Gay, P., 1965. Some crystallographic studies in the system $CaSO_4$–$CaSO_4 2H_2O$ I. The polymorphism of anhydrous $CaSO_4$. *Miner. Mag.*, **35**, 347–53.

Ghiorso, M., & Carmichael, I. S. E., 1981. A FORTRAN IV computer program for evaluating temperatures and oxygen fugacities from the compositions of coexisting iron-titanium oxides. *Computers & Geosci.* **7**, 123–9.

Gill, J. B., 1981. *Orogenic Andesites and Plate Tectonics*. Berlin-Heidelberg: Springer-Verlag, 390 pp.

Goff, F., Arney, B. H., & Eddy, A. C., 1982. Scapolite phenocrysts in a latite dome, northwest Arizona, U.S.A. *Earth planet. Sci. Lett.* **60**, 86–92.

Goldsmith, J. R., & Newton, R. C., 1977. Scapolite–plagioclase stability relations at high pressures and temperatures in the system $NaAlSi_3O_8$–$CaAl_2Si_2O_8$–$CaSO_4$. *Am. Miner.* **62**, 1063–80.

Haggerty, S. E., 1976. Opaque oxides in terrestrial igneous rocks. In: Rumble, D. (ed.) *Oxide Minerals*. Mineral. Soc. Am., 101–300.

Haughton, D., Roeder, P. L., & Skinner, B. J., 1974. Solubility of sulfur in mafic magmas. *Econ. Geol.* **69**, 451–67.

Hofmann, D. J., & Rosen, J. M., 1983. Stratospheric sulfuric acid fraction and mass estimates for the 1982 volcanic eruption of El Chichon. *Geophys. Res. Lett.* **10**, 313–16.

Huebner, J. S., & Sato, M., 1970. The oxygen fugacity-temperature relationships of the manganese oxide and nickel oxide buffers. *Am. Miner.* **55**, 934–52.

Katsui, Y., 1958. Groundmass anhydrite in the olivine basalt from the Rishiri volcano, Hokkaido. *J. Jap. Ass. Miner. Petrol. Econ. Geol.* **42**, 188–91.

Katsura, T., & Nagashima, S., 1974. Solubility of sulfur in magmas. *Geochim. cosmochim. Acta*, **38**, 517–31.

Krueger, A. J., 1983. Sighting of El Chichon sulfur dioxide clouds with the Nimbus 7 total ozone mapping spectrometer. *Science*, **220**, 1377–8.

Lovering, J. F., & White, A. J. R., 1964. The significance of primary scapolite in granulitic inclusions from deep-seated pipes. *J. Petrology*, **5**, 195–218.

Luhr, J. R., 1983. The 1982 eruptions of El Chichon and the relationship to mineralized magmatic-hydrothermal systems. *Geol. Soc. Am. Ann. Meeting Abstr.* 632.

—— Carmichael, I. S. E., & Varekamp, J. C. 1984. The 1982 eruptions of El Chichon volcano, Chiapas, Mexico: Mineralogy and petrology of the anhydrite bearing pumices. *J. Volcanol. geotherm. Res.* **23**, 69–108.

Mason, D. R., 1978. Compositional variations in ferromagnesian minerals from the porphyry copper-generating and barren intrusions of the western highlands. Papua New Guinea, *Econ. Geol.* **73**, 878–90.

Mathez, E. A., 1976. Sulfur solubility and magmatic sulfides in submarine basalt glass. *J. geophys. Res.* **81**, 4269–76.

Moore, J. G., & Fabbi, B. P., 1971. An estimate of the juvenile sulfur content of basalt. *Contr. Miner. Petrol.* **33**, 118–27.

Mroz, E. J., Mason, A. S., & Sedlacek, W. A., 1983. Stratospheric sulfate from El Chichon and the Mystery Volcano. *Geophys. Res. Lett.* **10**, 873–6.

Mysen, B. O., & Popp, R. K., 1981. Solubility of sulfur in $CaMgSi_2O_6$ and $NaAlSi_3O_8$ melts at high pressure and temperature with controlled f_{O_2} and f_{S_2}. *Am. J. Sci.* **280,** 78–92.

Nicholls, I. A., 1971. Calcareous inclusions in lavas and agglomerates of Santorini Volcano. *Contr. Miner. Petrol.* **30,** 261–76.

Newton, R. C., & Goldsmith, J. R., 1976. Stability of the end-member scapolites: $3NaAlSi_3O_8NaCl$, $3CaAl_2Si_2O_8$ $CaCO_3$, $3CaAl_2Si_2O_8$ $CaSO_4$. *Z. Kristallogr.* **143,** 333–53.

Nielsen, C. H., & Sigurdsson, H., 1981. Quantitative methods of electron microprobe analysis of sodium in natural and synthetic glasses. *Am. Miner.* **66,** 547–52.

Popadopolous, K., 1973. The solubility of SO_3 in soda-lime-silicate melts. *Phys. Chem. Glasses,* **14,** 60–5.

Popp, R. K., Nagy, K. L., & Hajash, A. Jr., 1984. Semiquantitative control of hydrogen fugacity in rapid-quench hydrothermal vessels. *Am. Miner.,* **69,** 557–62.

Prol, L., Medina, F., Choporov, D. Ya., Frikh, K., Muravitskaya, G. N., Polak, B. G., & Stepanets, M. I., 1982. Preliminary chemical and petrographic results of the March–April 'El Chichon' volcanics. *Geofis Int.* **21,** 1–10.

Rampino, M. R., & Self, S., 1982. Historic eruptions of Tambora (1815), Krakatau (1883), and Agung (1963), their stratospheric aerosols, and climatic impact. *Quaternary Res.* **18,** 127–43.

Robie, R. A., Hemingway, B. S., & Fisher, J. R., 1978. Thermodynamic properties of minerals and related substances at 298.15 K and 1 bar (10^5 Pascals) and at higher temperatures, *U.S. Geol. Surv. Bull.* **1452,** Washington: U.S. Govt. Printing Office.

Rose, W. I., Jr., Bornhorst, T. J., Hulson, S. P., Capaul, W. A., Plumley, P. S., Cruz-Reyna, S. de la, Mena, M., & Mota, R., 1984. Volcan El Chichon, Mexico: Pre-1982 S-rich eruptive activity, *J. Volcanol. geotherm. Res.* **23,** 147–67.

Rutherford, M. J., Sigurdsson, H., Carey, S., & Davis, A., 1985. The May 18, 1980 eruption of Mount St. Helens 1. melt composition and experimental phase equilibria. *J. geophys. Res.* **90,** 2929–47.

Rye, R. O., Luhr, J. R., & Wasserman, M. D., 1984. Sulfur and oxygen isotope systematics of the 1982 eruptions of El Chichon volcano, Chiapas, Mexico. *J. Volcanol. geotherm. Res.* **23,** 109–23.

Schneider, A., 1970. The sulfur isotopic composition of basaltic rocks. *Contr. Miner. Petrol.* **25,** 95–124.

Shaw, D. M., 1960. The geochemistry of scapolite. Part I. Previous work and general mineralogy. Part II. Trace elements, petrology, and general geochemistry. *J. Petrology,* **1,** 218–61.

Sigurdsson, H., 1982. Volcanic Pollution and climate: The 1783 Laki eruption. *EOS Trans. AGU,* **63,** 602.

Spencer, K. J., & Lindsley, D. H., 1981. A solution model for coexisting iron-titanium oxides. *Am. Mineral.* **66,** 1189–201.

Stormer, J. C., Jr., 1983. The effects of recalculation on estimates of temperature and oxygen fugacity from analyses of iron-titanium oxides. *Ibid.* **68,** 586–94.

——Carmichael, I. S. E., 1971. The free energy of sodalite and the behavior of chloride, fluoride, and sulfate in silicate magmas. *Ibid.* **56,** 292–306.

Stull, R., & Prophet, H., 1971. *Joint Army Navy Air Force Thermochemical Tables,* 2.

Taylor, G. A., 1958. The 1951 eruption of Mount Lamington, Papua. *Bureau Miner. Resources Geol. Geophys. Bull.* **38,** 1–117.

Tracy, R. J., & Hummel, H., 1981. Zoned hauyne phenocrysts in Tahitian phonolitic lavas. *Geol. Soc. Am. Ann. Meeting Abstr.* 537.

Ueda, A., & Sakai, H., 1984. Sulfur isotope study of quaternary volcanic rocks from the Japanese Island Arc. *Geochim. cosmochim. Acta,* **48,** 1837–48.

Varekamp, J. C., Luhr, J. F., & Prestegaard, K. L., 1984. The 1982 eruptions of El Chichon volcano (Chiapas, Mexico): Character of the eruptions, ash-fall deposits, and gas phase. *J. Volcanol. geotherm. Res.* **23,** 39–68.

Wendlandt, R. F., 1982. Sulfide saturation of basalt and andesite melts at high pressures and temperatures. *Am. Miner.* **67,** 877–85.

Whitney, J. A., 1984. Fugacities of sulfurous gasses in pyrrhotite bearing silicic magmas. *Ibid.* **69,** 69–78.

——Stormer, J. C., 1983. Igneous sulfides in the Fish Canyon Tuff and the role of S in calc-alkaline magmas. *Geology,* **11,** 99–102.

Williams, D. W., 1968. Improved cold seal pressure vessels to operate to 1100°C at 3 kilobars. *Am. Miner.* **53,** 1765–69.

Yagi, K., Takeshita, H., & Oba, Y., 1972. Petrological study of the 1970 eruptions of Akita-Komagatake Volcano, Japan. *Japan. Jour. Fac. Sci. Hokkaido Univ. Ser IV* **15,** 109–38.

Yoshiki, 1938. Activity of Akita–Komagatake Volcano. *J. Japan. Ass. Min. Petrol. Econ. Geol.* **9,** 153–60.